Environ Monit Assess (2013) 185:1215–1235
DOI 10.1007/s10661-012-2627-8

A new multiscale approach for monitoring vegetation using remote sensing-based indicators in laboratory, field, and landscape

Angela Lausch · Marion Pause · Ines Merbach · Steffen Zacharias · Daniel Doktor · Martin Volk · Ralf Seppelt

Received: 11 October 2011 / Accepted: 2 April 2012 / Published online: 25 April 2012

Abstract Remote sensing is an important tool for studying patterns in surface processes on different spatiotemporal scales. However, differences in the spatiospectral and temporal resolution of remote sensing data as well as sensor-specific surveying characteristics very often hinder comparative analyses and effective up- and downscaling analyses. This paper presents a new methodical framework for combining hyperspectral remote sensing data on different spatial and temporal scales. We demonstrate the potential of using the "One Sensor at Different Scales" (OSADIS) approach for the laboratory (plot), field (local), and landscape (regional) scales. By implementing the OSADIS approach, we are able (1) to develop suitable stress-controlled vegetation indices for selected variables such as the Leaf Area Index (LAI), chlorophyll, photosynthesis, water content, nutrient content, etc. over a whole vegetation period. Focused laboratory monitoring can help to document additive and counteractive factors and processes of the vegetation and to correctly interpret their spectral response; (2) to transfer the models obtained to the landscape level; (3) to record imaging hyperspectral information on different spatial scales, achieving a true comparison of the structure and process results; (4) to minimize existing errors from geometrical, spectral, and temporal effects due to sensor- and time-specific differences; and (5) to carry out a realistic top- and downscaling by determining scale-dependent correction factors and transfer functions. The first results of OSADIS experiments are provided by controlled whole vegetation experiments on barley under water stress on the plot scale to model LAI using the vegetation indices Normalized Difference Vegetation Index (NDVI) and green NDVI (GNDVI). The regression model ascertained from imaging hyperspectral AISA-EAGLE/HAWK (DUAL) data was used to model LAI. This was done by using the vegetation index GNDVI with an R^2 of 0.83, which was transferred to airborne hyperspectral data on the local and regional scales. For this purpose, hyperspectral imagery was collected at three altitudes

A. Lausch (✉) · D. Doktor · M. Volk · R. Seppelt
Department of Computational Landscape Ecology,
UFZ—Helmholtz Centre for Environmental Research,
Permoserstr. 15,
04318 Leipzig, Germany
e-mail: Angela.Lausch@ufz.de

M. Pause
Water & Earth System Science Competence Centre,
University of Tuebingen,
Keplerstrasse 17,
72074 Tuebingen, Germany

I. Merbach
Department of Community Ecology,
Helmholtz Centre for Environmental Research—UFZ,
Theodor-Lieser-Str. 4,
06120 Halle, Germany

S. Zacharias
Department Monitoring & Exploration Technologies,
Helmholtz Centre for Environmental Research—UFZ,
Permoserstr. 15,
04318 Leipzig, Germany

over a land cover gradient of 25 km within a timeframe of a few minutes, yielding a spatial resolution from 1 to 3 m. For all recorded spatial scales, both the LAI and the NDVI were determined. The spatial properties of LAI and NDVI of all recorded hyperspectral images were compared using semivariance metrics derived from the variogram. The first results show spatial differences in the heterogeneity of LAI and NDVI from 1 to 3 m with the recorded hyperspectral data. That means that differently recorded data on different scales might not sufficiently maintain the spatial properties of high spatial resolution hyperspectral images.

Keywords Hyperspectral remote sensing · Spatiotemporal scale · Controlled long-term laboratory experiment · Imaging spectroscopy · Semivariogram · AISA-EAGLE/HAWK (DUAL)

Introduction

The scale is a basic concept for describing the hierarchical structure of landscapes, structures, and processes. With the development of remote sensing techniques for different spatial and spectral resolutions, scale issues and questions concerning scale transitions became one of the focal research topics of scientists. Although a number of methods have been applied in remote sensing for multiscale analysis in landscape ecology, the effectiveness of many of these, including some of the more commonly used ones, is not always apparent and sometimes questionable. To our knowledge, there is no universal method in remote sensing for calculating the effects of different scales, methods of scaling, and scale transitions. Each method has its specific problems, limitations, and certain conditions. The methods applied depend on the available data products, the various geometric and spectral resolutions and the existing limitations of the data used. According to Wu (2009), the reasons why no single method has been proven to be effective can be put down to the following criteria: (1) the heterogeneity of the landscape surface and objects, (2) the nonlinearity of retrieval models, and (3) different targets. Wu (2009) points out that the research on scale and scale effects in remote sensing is still at the very beginning. Wu (2009) summarizes four essential reasons for the difficult transfer of information over different scales: (a) different instruments have different fields of view (FOV) that correspond to different spatial resolutions; (b) instruments of a comparable target measurement have a different technical design and acquisition parameters; (c) the scale at which models operate often varies from model to model; and (d) different factors, such as funding, the time of data recording and manpower constrain the choice of scale, the mode, and the intensity of measurements.

There are many different definitions of scaling (Meentemeyer 1989; Gibson et al. 2000; Dungan 2001; Wu 2009); but for remote sensing data, the scaling definition after Quattrochi (1993) is most relevant. According to Quattrochi (1993), the scale of optical imaging data is "the combination of space, electromagnetic wavelengths, their direction, and the time intervals over which a spectrometric measurement is made". When considering new methods of scaling techniques, we have to deal with new approaches in up- and downscaling. In this respect, the bottom-up approach—transferring information from smaller to larger scales of observation—is referred to as upscaling, whereas the top-down approach "downscales" information from a larger to a smaller scale (Volk and Ewert 2011). In optical remote sensing, different techniques can be employed to perform up- or downscaling, which are widely applied and accepted in the research field of spectroscopy. These are (1) radiative transfer modeling, (2) spectral (un) mixing, and (3) data fusion techniques. Malenovský et al. (2007) demonstrate the scaling abilities for top- and/or downscaling for spatial, spectral, directional, and temporal scale optical remote sensing techniques (Table 1).

What exactly are the specific problems involved in using the existing methods for up- and downscaling in remote sensing? In the following, three common methods are discussed.

Radiative transfer models for scaling Radiative transfer models (RTM) are physical approaches for scaling the spatial, spectral, and directional information of landscape surfaces and observation objects. They can range from simple 1D models for modeling purely homogenous canopy structures to horizontally heterogeneous or discontinuous vegetation canopy models such as the Discrete Anisotrophic Radiative Transfer (DARD) models (Myneni 1991; Myneni and Ganapol 1991; Gastellu-Etchegorry et al. 2004). RTM are

Table 1 Scaling abilities for top-and/or downscaling of the remote sensing techniques described (modified from Malenovský et al. (2007))

Scale dimension	Direction	Radiative transfer Models (RTM)	Spectral (Un)mixing	Data merging	OSADIS
Spatial	Upscaling	++	–	++	++
	Downscaling	–	++	–	++
Spectral	Upscaling	+	–	–	++
	Downscaling	–	–	–	++
Directional	Upscaling	+	–	–	–
	Downscaling	–	–	–	–
Temporal	Upscaling	–	–	–	++
	Downscaling	–	–	++	++

– Scaling has not been investigated or is impossible; + there are examples for this scaling dimension, but with limitations; ++ there are good examples for this scaling dimension

designed for scaling spectral derivatives and testing different spectral indices with different spatial, spectral, and directional resolutions. Spectral indices such as the Normalized Difference Vegetation Index (NDVI; Lillesand and Kiefer 1994) and others are designed to describe the properties and detected changes in biochemical and physical properties of observed vegetation and landscape objects. Not all spectral indices on the leaf level are directly applicable on the next spatial scale of the canopy because of the heterogeneity and geometry of the environment. Haboudane et al. (2002) combined the leaf RT model PROSPECT (Jacquemoud et al. 2009) with the canopy RT model SAIL (Verhoef 1984) to test the ratio of two spectral indices (Haboudane et al. 2008; Li et al. 2008). A further combination with a 3D geometry model such as DARD would also be possible although its application is difficult because limitations arise due to the high complexity and heterogeneity of the vegetation and the landscape. Gascon et al. (2004) used the DART model to simulate images of a tropical forest at 1 and 50 m ground resolution. However, the results of the Leaf Area Index (LAI) modeling and the NDVI were very different. This example demonstrates that a retrieval of biochemical–physical variables using RT modeling is possible, but must be correctly adapted at a very high spatial resolution (Malenovský et al. 2007). RT models "are not designed for any downscaling" techniques and for the temporal scaling dimension. The RTM present a tremendous opportunity in terms of their abilities for spatial, spectral, and directional scaling but the reflectance of leaf, canopy, and landscape objects is a complex system of different scale dimensions. Hence, the correct parameterization of the RT models is particularly important. Due to the large number of possible input parameters for RT models, the exact parameterization is still the limiting factor, or at least the area with the highest errors. More specific information and state-of-the art in theory and application of RTM are available in Schönermark et al. (2004).

Spectral (un)mixing for scaling Spatial homogeneity is a rare phenomenon for the surface of landscapes. Usually, one or more substances or objects provide spectral information for an image pixel. The reflectance value R of a pixel depends on the optical and structural properties of both the surface and landscape objects. The optical and structural properties as well as the homogeneous or heterogeneous character of the surface and landscape object determine whether the mixing process is linear or nonlinear (Malenovský et al. 2007; Wu 2009). Smith et al. (1985) were the first to develop a method for the spatial downscaling of remote sensing data—the spectral mixture analysis (SMA). SMA is used to find the fractions or the abundance of a number of surface elements (end members) that explain the recorded mixed pixel reflectance spectrum. There are different methods for the "end member" selection such as using spectral libraries modeled with RTM (Painter et al. 2003) using field spectra from field measurements or image-derived "end members" from the purest pixels of the spectral image. The different techniques for automated image

end member selection have been published by Dennison and Roberts (2003). Spectral (un)mixing techniques have been realized in different fields of image spectroscopy using different kinds of optical remote sensing data. Painter et al. (2003) for example applied a multiple "end member" SMA to AVIRIS data for analyzing snow cover areas while Metternicht and Zinck (2003) used SMA for soil salinity with the DAIS sensor.

Merging data for scaling There are many optical sensors with different characteristics in the spatial, spectral, temporal, or directional dimension. The aim of data fusion techniques is therefore to combine the information from a multisource dataset for spatial and temporal downscaling. Traditionally, image fusion techniques use an image with a low spatial resolution (multispectral image) for downscaling to a higher spatial resolution image with a higher panchromatic image. A number of merged examples can be found with LANDSAT TM and SPOT images (Zhou et al. 1998), QUICKBIRD, IKONOS, and HYPERION (Zeng et al. 2009), or the merging of hyperspectral data such as AISA and multispectral LANDSAT ETM images (Chen et al. 2003; Silvan-Carrdenas and Wang 2010). Several statistical approaches have been used for the implementation of fusion algorithms such as the wavelet transformation (Zhou et al. 1998; Li et al. 2002; Saunders et al. 2005), the intensity–hue–saturation transformation, the principal component analysis, the Ranchin transformation (Zhou et al. 1998; Ranchin et al. 2003) and different machine learning techniques (Tuia et al. 2009). For temporal scaling or vegetation monitoring, there are many different data fusion approaches available, dealing with different spatial and/or temporal scale dimensions. The global NDVI are derived from advanced very high resolution radiometer (AVHRR), SPOT-VGT, and MODIS earth observation data (Tarnavsky et al. 2008), for the global monitoring of the environment and vegetation SPOT-4/-5/IRS, AVHRR/MSG, ASTER, IKONOS/QuickBird/OrbView/GeoEye, and DMC/SPOT-1/-2 Imagery Part II are used (Baraldi et al. 2010; Gobron et al. 2010).

All of the aforementioned processes and methods cover individual areas of up- or downscaling of spatial, spectrodirectional, or temporal aspects. Temporal upscaling, the investigation of the spectral response of structures, functions, and processes over time, is currently not covered by any of the methods described above.

The objectives of the study presented here are: (1) to develop, test, and apply a new methodical framework for combining hyperspectral remote sensing data on different spatial and temporal scales to monitor vegetation variables on plot, local, regional, and global scales; (2) to transfer the modeling results obtained from the long-term laboratory experiment to the local/regional scale to hyperspectral data with differently recorded geometrical spatial resolutions from 0.5 to 3 m; (3) to carry out analyses to compare the spatial heterogeneity of hyperspectral data with differently recorded soil/ground resolutions of 0.5–3 m; and finally, (4) to illustrate the potential of using one sensor at different scales to monitor vegetation properties.

A methodological framework for multiscale analysis

The monitoring of vegetation and land surface variables at different scales can be realized through an approach that will be applied in this paper—the "One Sensor at different Scales" Approach (OSADIS). In this approach, the same hyperspectral sensor is used at three different observation scales scale 1 (plot scale), scale 2 (local scale), and scale 3 (regional scale), which are presented in Fig. 1. Scales 1–3 are outlined in more detail in the following section, whereas scale 4 (the global scale) will not be discussed in this paper.

For the OSADIS approach, we used the imaging spectrometer sensors: AISA-EAGLE (400–970 nm) and AISA-HAWK (970–2,500 nm). AISA stands for Airborne Imaging Spectrometer for Applications (Mäkisara et al. 1993) developed by SPECIM (Spectral Imaging LTD., Finland). Table 2 summarizes the main properties of the imaging spectrometers that are being used. The relevant spectral and geometric sensor properties required are set according to the research objectives and the scale of the spatial observation. The permanent availability of the sensors guarantees data acquisition at any required time on the landscape scale using different aircraft.

Experimental design

Scale 1. The plot scale—monitoring experiment of the complete plant cycle in the laboratory

In order to investigate the plot scale, the AISA imaging hyperspectral sensors were used in the laboratory.

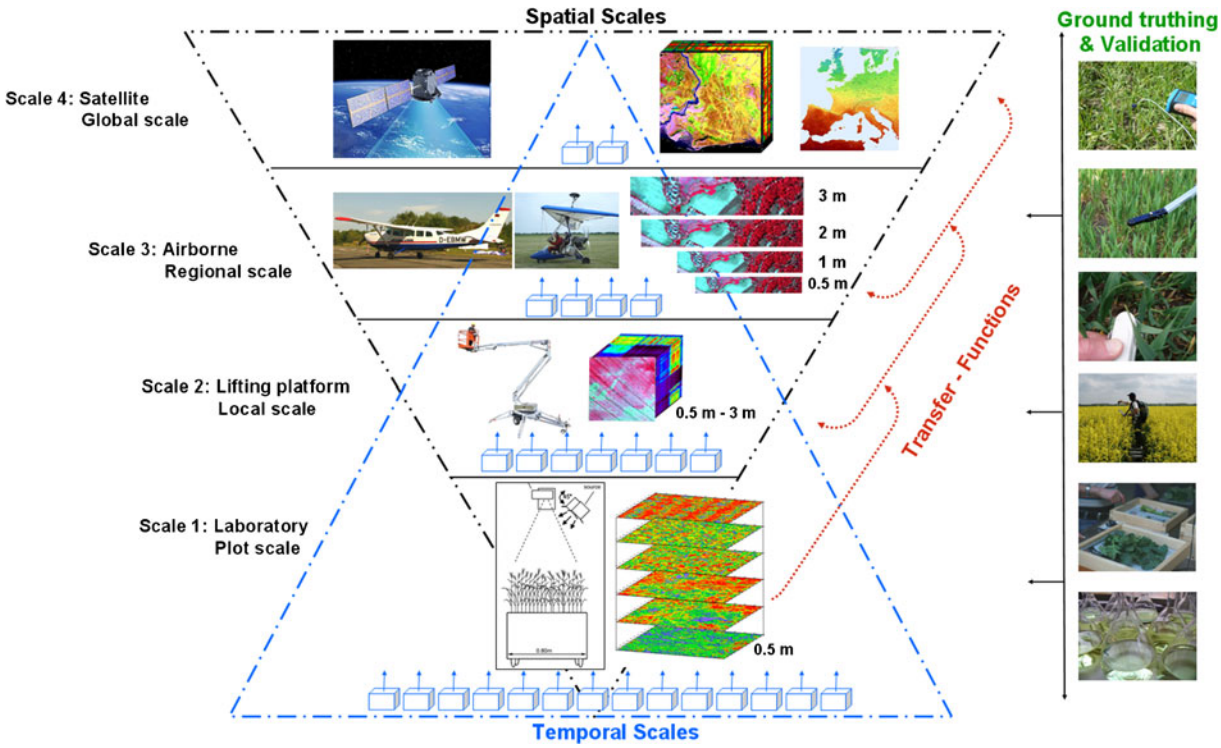

Fig. 1 The basic concept of monitoring the biophysical variables of vegetation on different spatial and temporal scales with the imaging hyperspectral sensors AISA-EAGLE/HAWK (DUAL)

Table 2 Characteristics of the imaging hyperspectral sensors AISA-EAGLE/HAWK, SPECIM (Spectral Imaging LTD, Finland)

Sensor head	AISA-EAGLE VNIR				AISA-HAWK II SWIR
Mass	11 kg				18 kg
Dimensions (L/W/H)	380/220/55 mm				220/275/470 mm
Spectral range	400–970 nm				970–2,500 nm
Spectral resolution	2.9 nm				8.5 nm
Spatial pixels, up to	1,024				320
Camera	CCD camera				MCT camera
SNR	350:1–1,400:1 (depend on band configuration)				800:1 (peak)
Spectral binning options	1×	2×	4×	8×	
Spectral bands	488	252	122	60	254
Spectral sampling/band	1.25 nm	2.3 nm	4.6 nm	9.2 nm	
Image rate	30	40	60	85	
Focal length	23x mm	18.5 mm		9 mm	22.5 mm
FOV	29.9°	36.7°		62.1° degree	24.0° degree
Swath width	0.53× altitude	0.66× altitude		1.20× altitude	0.43× altitude
Ground resolution at 1,000 m altitude	0.52 m	0.65 m		1.2 m	1.34 m
Additional parts for Eagle and Hawk					
Mirror scanner	Mirror scanner for local applications (field plots)				
FODIS	Fiber optic down welling irradiance sensor				

The AISA EAGLE/HAWK (DUAL) imaging hyperspectral sensors were mounted on a lifting-platform at a height of 2.6 m above the ground (Fig. 2). In front of both AISA sensors' optical lenses, the rotating mirrors were installed to guide the illumination to the sensors line and to retrieve imaging data. A dark room of approximately 4×4 m made of lightproof material was constructed for the hyperspectral measurements. The use of this kind of darkroom prevents any disruptive factors from having an effect over the entire series of tests. Light was provided from artificial light sources using 2000-W tungsten–halogen–quartz lamps (Kaiser StudioLight, Kaiser Fototechnik, Buchen, Germany). The observation height was set at 2 m above the canopy of plant material. A spectralon reflectance panel (61×61 cm, Spectralon SRT-99-240, Labsphere, Inc.) was placed directly above the vegetation sample container at the beginning of each measurement scan. The leaf sample container and the white reference were irradiated under the same light conditions. Using the spectral reflectance factors of the spectralon target enabled the radiance that was reflected from the vegetation sample to be calculated.

For comparison with the AISA imaging spectrometer data, non-imaging hyperspectral data was collected using the ASD FieldSpec 3 (Analytical Spectral Device, Inc., Boulder, CO, USA). The ASD spectrometer (350–2,500 nm, 2,150 spectral channels, 1.4–2 nm spatial resolution) was mounted at the same height as the scanning spectroradiometer AISA with a FOV of 8°. For the ASD, we used a conversion lens with a FOV of 8° to sample a vegetation plot of 30×30 cm.

To determine the plant physiological and biochemical status, chlorophyll content (Minolta SPAD 502 Chlorophyll meter, Spectrum Technologies, Plainfield, IL, USA), leaf area index (LAI, LAI 2000 Plant Canopy Analyzer, Li-Cor, Lincoln, NE, USA), chlorophyll fluorescence parameters (Mini-PAM, pulse amplitude modulated fluorometer, Walz, Germany) plant height, biomass, leaf water content, C and N content, soil moisture (theta probes), and matrix potential measurements were taken in addition to hyperspectral data acquisition. Laboratory measurements such as temperature, radiation intensity, air humidity, and observations of soil moisture and matrix potential were recorded hourly.

Different plants such as summer barley (*Hordeum vulgare* L), rapeseed (*Brassica napus*), wheat (*Triticum* spec.) European ash (*Fraxinus excelsior*), spruce (*Picea abis*), and rape (*B. napus*) were exposed or not exposed (for control purposes) to different stress scenarios (drought and flood stress) either over the entire vegetation period or over a 3–5 months vegetation period. Over this vegetation period, all spectral (imaging hyperspectral data—AISA-EAGLE/HAWK, non-imaging ASD spectrometer) and vegetation parameter measurements were taken twice a week. Soil and climate parameters were recorded hourly in the climate chamber.

Scale 2. The field scale using a lifting platform

The next scale level (scale 2) represents the local scale. The respective test plots reflecting field conditions with an observation extent of approximately 20×20 m were examined using a lifting platform. The hyperspectral sensors (AISA-EAGLE/HAWK) were mounted on the lifting platform at various altitudes (2–12 m) above the vegetation canopy. The aim of

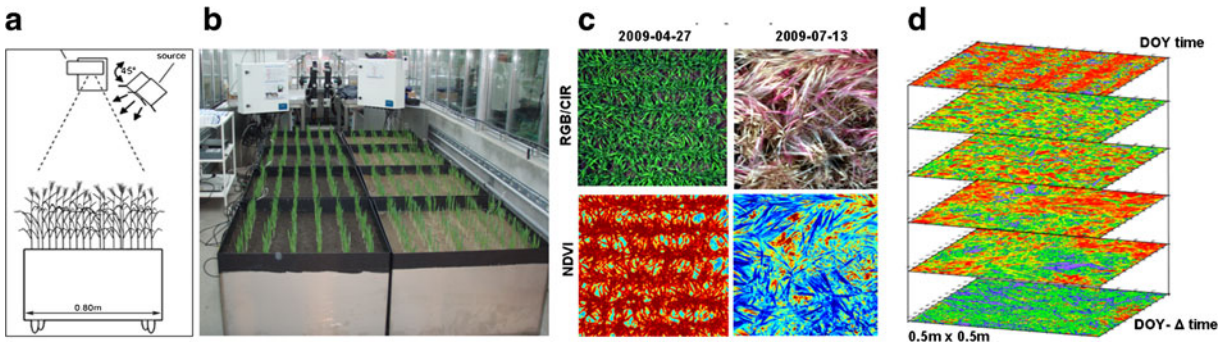

Fig. 2 The use of imaging hyperspectral sensors AISA-EAGLE/HAWK (DUAL) in the laboratory experiment; **a** technical configuration of the hyperspectral sensors, **b** controlled vegetation scenarios of the spring barley experiment 2009, **c** RGB/CIR and NDVI derived from the AISA-EAGLE hyperspectral image from spring barley (April 27 to July 13, 2009), **d** NDVI from different DOY. Time period, April 27 to July 20, 2009

these experiments was to record the causal relationships between spectral imaging hyperspectral signals (reflectance and radiance) and the target parameters measured (e.g., to derive biophysical and biochemical canopy state variables such as LAI, pigment content, vegetation water content, and nutrient status) under field conditions. The lifting platform enables tests to be conducted on the influence of different sensor angles, the bidirectional reflectance distribution function (BRDF) effects on the spectral response of imaging, and the definition of transfer functions of the spectral response from scale 1 (laboratory) to scales 2 (local) and 3 (regional).

Scale 3. The local and regional scale—airborne remote sensing

To provide airborne hyperspectral imaging data for innovative studies, we used a microlight aircraft (Trike, D-MUFZ) for small-scale hyperspectral campaigns (Fig. 3) and a Cessna 207 or Piper for extensive hyperspectral campaigns (Fig. 4) as a sensor platform. Figure 3 shows the hyperspectral sensor AISA-EAGLE together with a GPS/INS unit RT3100 (Oxford Technical Solutions LTD., UK) mounted onto the microlight aircraft as well as the aircraft itself in operation.

The availability of the sensor (AISA-EAGLE/HAWK) and the microlight aircraft as an additional platform for a sensor in addition to a Cessna or Piper airplane enable a very flexible application. Depending on the area size and the monitoring rate of our study sites, we selected the appropriate platform (microlight aircraft or Cessna, Piper) for the sensor. Our "OSADIS Approach" implies that all hyperspectral airborne surveys will be flown at different spatial scales with ground resolutions of 0.5–3 m within a very short time frame (approximately 2–3 h).

Methodology and data processing of the multiscale approach

The approach described for combining hyperspectral information on different spatial and temporal scales into a unified set of spectral data is provided in Fig. 5.

The procedure for hyperspectral data on the plot scale Over the entire vegetation period, all imaging hyperspectral data (AISA-DUAL) were taken twice a week for specific selected field crop vegetation. To minimize the influences of factors such as radiation and geometry over the entire measurements, we always used the same measurement design (see "Experimental design" section). After being recorded, radiometric corrections were performed on the hyperspectral data based on the procedure CaliGeo (Spectral Imaging Ltd; Mäkisara 1998) run under ENVI (ITT Visual Information Solution, Boulder, CO, USA). The semi-atmospheric corrections and the transformation of radiances to reflectances were carried out using a spectralon reflectance panel (61×61 cm, Spectralon SRT-99-240, Labsphere, Inc.) using a procedure after Carter (1994). The semigeometric correction was realized using a master–slave geometric correction approach under ENVI. After preprocessing, the hyperspectral data are referred to as ground reflectance data with a spatial ground resolution of 0.2 cm and a FOV of 0.5×0.5 m. These datasets provide hyperspectral information input for different semi-empirical and empirically based remote sensing techniques (i.e., vegetation indices, spatial variability indicators, physical-based–RT models PROSPECT; Jacquemoud et al. 2009) SAIL (Verhoef 1984) and different classification approaches. Additionally, the ground reflectances are the base for an imaging spectral library and for different classification approaches.

For comparison with the AISA EAGLE/HAWK imaging spectrometer data, non-imaging hyperspectral data were collected using ASD FieldSpec 3 (Analytical Spectral Device, Inc.).

The procedure for hyperspectral data on the local, regional, and global scale To keep the disturbing influences from radiation and geometry factors of vegetation (BRDF) as low as possible, the hyperspectral images were recorded with a ground resolution of 0.5, 1, 2, and 3 m for the same land cover gradient or other test sites. The time intervals between the recorded datasets were about 60 min.

After recording the airborne AISA-EAGLE/HAWK raw data were radiometric-corrected based on the procedure CaliGeo (Spectral Imaging Ltd; Mäkisara 1998) run under ENVI (ITT Visual Information Solution). After the radiometric correction, ocular linear, and nonlinear miscalibrations in the hyperspectral data were reduced by implementing an image-driven, radiometric recalibration and rescaling method (Reduction of miscalibration effects; Rogaß et al. 2011). The atmospheric correction was performed using the

Fig. 3 **a** AISA-EAGLE (400–970 nm) and GPS/INS-RT3100 mounted on the UFZ's microlight aircraft (Trike), **b** the UFZ's microlight aircraft (D-MUFZ), **c** "Schleusenheger Wiesen" near Dessau recorded on July 3, 2008 with the UFZ's microlight aircraft, images from the hyperspectral sensor AISA-EAGLE, 400–970 nm, 1 m ground resolution, 252 spectral bands, CIR-AISA-EAGLE hyperspectral image with data cube

software procedure ATCOR4 (Richter and Schlapfer 2002) and the radiative transfer in ATCOR. The program corrects at-sensor radiance images for solar luminance, aerosol scattering, and the Raleigh. The ATCOR program has been adapted for the specific band characteristics of the AISA-EAGLE/HAWK sensors. The orthorectification of the airborne hyperspectral image was carried out using a digital elevation model together with the geocoding procedure CaliGeo.

After preprocessing, the hyperspectral data were referred to as ground reflectance data with the different spatial ground resolutions of 0.5, 1, 2, and 3 m. These spatially very different datasets can serve as input data for many semi-empirical and empirical remote sensing techniques such as vegetation indices, physically based models RT models, i.e., PROSPECT (Jacquemoud et al. 2009), SAIL (Verhoef 1984), and analytical methods such as the principal components analysis or spectral unmixing methods etc. Due to the approach of only using one sensor (AISA-DUAL), a spectral harmonization is not necessary. The geometric characteristics for the 0.5, 1, 2, and 3 m images of the hyperspectral data are different. To investigate scaling effects, hyperspectral data were recorded at the local and regional level with different spatial resolutions (c.f. Fig. 1). The

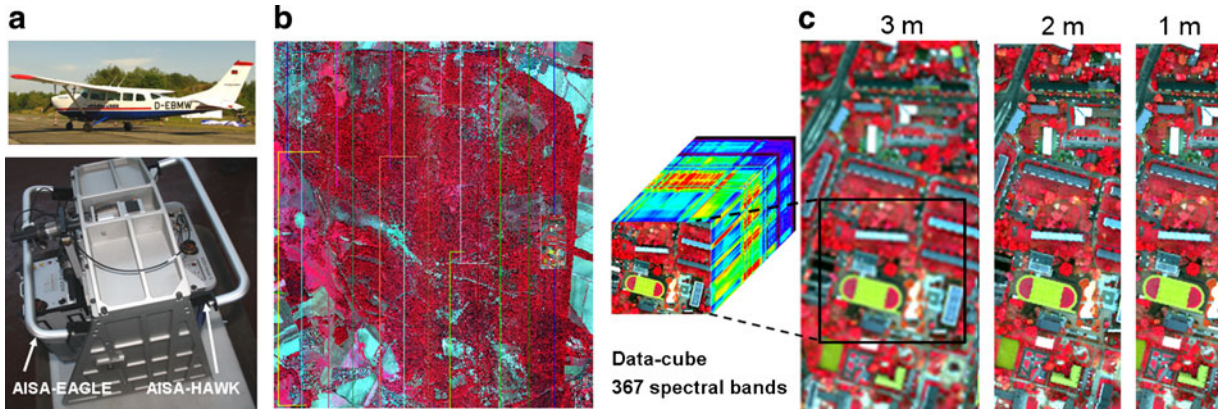

Fig. 4 **a** AISA-Eagle/HAWK Dual sensor mounted on Cessna 207, **b** "Döberitzer Heide" near Berlin, CIR-image from a hyperspectral sensor on the AISA-EAGLE, 400–970 nm swath-mosaic, 2 m ground resolution, 252 spectral bands, date of recording August 16, 2009 with a Cessna 207, **c** Cottbus, CIR-image from hyperspectral sensors of the AISA-EAGLE/HAWK (AISA-DUAL) 400–2,500 nm with data cube, 367 spectral bands with 1, 2, 3 m recorded ground resolution, date of recording October 20, 2009 with a Cessna 207

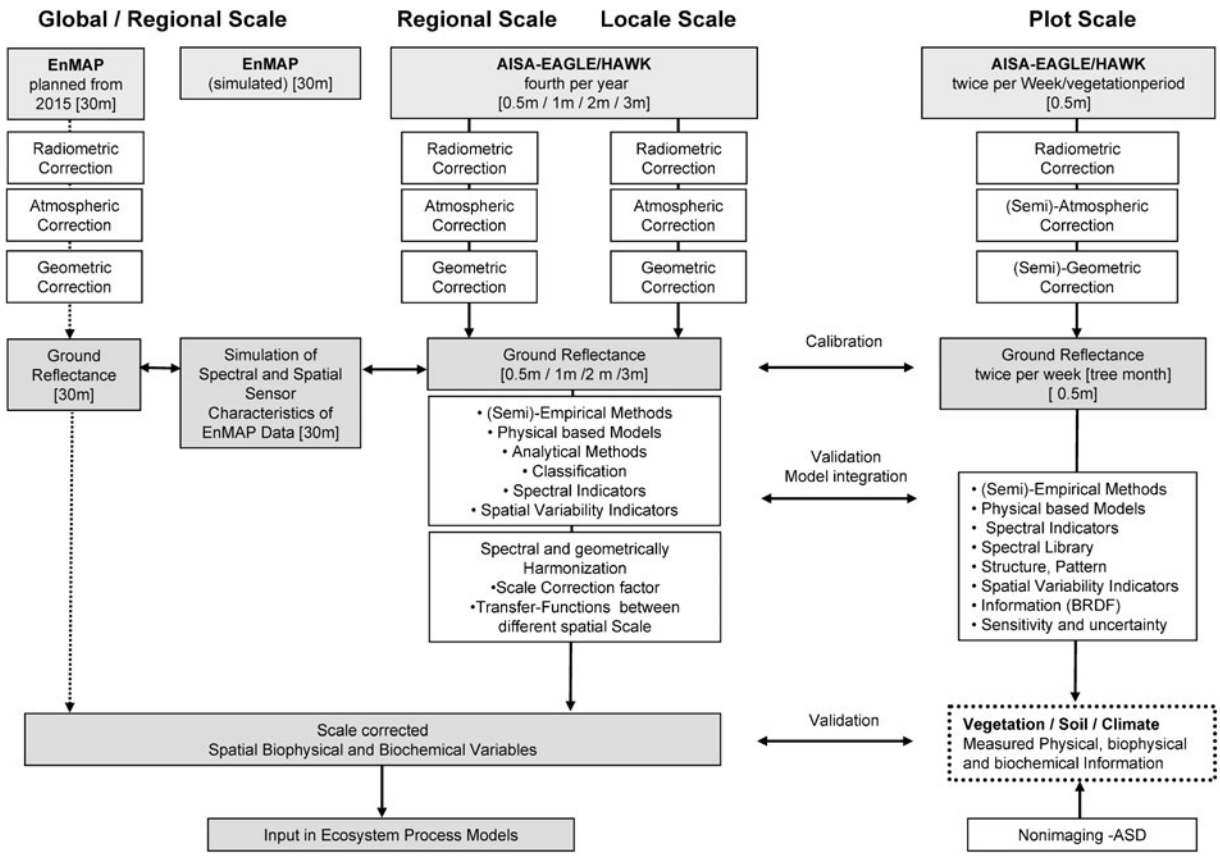

Fig. 5 Flowchart of the OSADIS approach for a long-term multiscaling analysis on different scales (plot, local, regional, and global)

differences in the geometric ground resolutions are harmonized using methods that integrate scale correction factors or transfer functions between different spatial scales.

The information that is retrieved from the corrected spatial biophysical and biochemical vegetation parameters is validated against the measurements from the ground truth data of the plot-scale experiment and the direct measurements from ground truth data in the field. The verified spatial information from the hyperspectral remote sensing data is used as a base dataset for different ecosystem process models.

The transfer of statements from the regional scale to the global scale requires the implementation and use of spaceborne hyperspectral sensors with a wider swath. The hyperspectral sensor Environmental Mapping and Analysis Program (EnMAP)—that will be launched in 2015—fulfills these requirements. To transfer hyperspectral information from the regional to the global scale based on the ground reflectance data (3 m) of the AISA-EAGLE/HAWK hyperspectral sensors, a simulation is carried out of the geometric (30 m) and spatial (400–2,500 nm) sensor characteristics of the EnMAP Hyperspectral Sensor with a scene simulator for optical earth observation data (Guanter et al. 2009; Segl et al. 2010a, b). The implementation of this method enables a comparison and a coupling of different geometrical spectral characteristics that can be integrated into local, regional, and global ecosystem models.

Implementation of the OSADIS experimental setup

Study area and data

Study area The study area for the experiments is part of the Terrestial Environmental Observatories (TERENO) long-term monitoring region (www.tereno.net, Zacharias et al. 2011), situated in the Harz region in Central Germany (Fig. 6). Imaging was carried out using the hyperspectral sensors along a 25 km land use gradient at four different points in time within a

Fig. 6 Study area for recording imaging hyperspectral data from the AISA-EAGLE/HAWK (DUAL) sensor, land cover gradient of 25 km situated in the Harz mountains in central Germany

vegetation period with a ground resolution of 1, 2, and 3 m. To maximize any differences in illumination, BRDF as well as phenological and biophysical differences in the vegetation, the imagery was taken within a short time frame of 60 min on the same day. This ensures the greatest comparability of hyperspectral information with different ground resolutions of 1, 2, and 3 m.

The specifications for recording hyperspectral data for the controlled laboratory experiment as well as the hyperspectral data recorded on the aircraft platform are described in Table 3

For our investigation, the following land surface variables are important The NDVI is an expression of reflectance between red and near-infrared regions of a surface spectrum (Rouse et al. 1973). The NDVI is directly related to general greenness (Sellers 1985), biomass, vegetation abundance, and structures of the vegetation and is expressed as:

$$\mathrm{NDVI} = (\mathrm{R800} - \mathrm{R670})/(\mathrm{R800} + \mathrm{R670}) \quad (1)$$

The NDVI is a renowned and very frequently used vegetation index. There are several variations in the way in which the NDVI is used, but for this study we used the reflectance values at a wavelength of 680 nm as red and 800 nm as NIR.

The green NDVI (GNDVI) developed by Gitelson et al. (1996) is an index for chlorophyll estimation. The index should be invariant with respect to other pigments other than chlorophyll and should not be influenced by other external factors such as the background or the atmosphere (Bannari et al. 2007). It is expressed as:

$$\mathrm{GNDVI} = (\mathrm{R800} - \mathrm{R550}) \quad (2)$$

The LAI is an important structural and biophysical parameter of vegetation canopies that is specifically coupled with other canopy variables (e.g., crop yield, above-ground biomass, and ground coverage). The LAI is therefore an appropriate indicator of crop growth over the entire phenological growing season. The LAI assessment is important as an input variable for many ecological, hydrological, or climatological modeling approaches. The LAI is used as an input variable in numerous ecological models. For this reason, modeling LAI from remote sensing data is an important prerequisite as an input variable in ecological process

Table 3 Parameters of the recorded imaging and non-imaging hyperspectral data

Recording date	Recording ground resolution (m)	Focal length	FOV (degree)	Swath (m)	Spectral range (nm)	Spatial pixel	Spectral resolution (nm)	Spectral bands	Sesor	Platform
3 Months twice a week (April 27 to April 20)	0.025	18.5	36.7	0.5×0.5	400–970	512	2.5–3.0	252	AISA-EAGLE	Laboratory
		22.5	24.0	0.5×0.5	970–2,400	320	6.30	237	AISA-HAWK	
June 16, 2010	1	18.5	36.7	512	400–2,400	300	4.2–4.8	107	AISA-EAGLE	Aircraft—Cessna 206
June 16, 2010	3	18.5	36.7	1,536	400–2,400	300	4.2–4.8	107	AISA-EAGLE	Aircraft—Cessna 206
September 9, 2010	1, 2, 3	18.5/22.5	36.7	300	400–2,400	300	4.25–6.26	491	AISA-EAGLE/HAWK (DUAL)	Aircraft—Cessna 206
3 Months twice a week (April 27 to July 20, 2009)	–		8	0.3×0.30	350–2,400	–	1.4–2	2,150	ASD-FieldSpec 3	Laboratory/field

models. The LAI was derived by regression analysis between the LAI sensor (LAI2000) and the vegetation index GNDVI for the plot scale. This regression analysis was used for modeling the LAI on the local and landscape scales (Figs. 9 and 10).

Analysis of heterogeneity

One index for characterizing the spatial heterogeneity (patchiness) of abiotic and biotic patches or vegetation indices (NDVI) and therefore the direction and extent of spatial processes is defined by the correlation length (Isaak and Srivastava 1989; Ettema and Wardle 2002). The correlation length is based on the variogram $\gamma(h)$, which is usually estimated from the experimental variogram.

$$\gamma(h) = \left(1/2n(h)\mathrm{sum}[z(xi+h) - z(xi)]\right)^{\wedge}2 \quad (3)$$

In Eq. (3) the $z(xi + h)$ are the data or measurement points at locations x and $x + h$, where h is the distance or lag between two data or measurement points, and $z(xi)$ are the number of pairs of measurement points with distance h.

The semivariance tests whether the similarity between densely spaced points is greater than points that are more distant from one another (Webster and Oliver 2001). With range, autocorrelation length, or the gradient (Fig. 7), the distance is indicated from which two measurement values show no correlation with each other. It is taken from the variogram at the point where the variogram value of the best-fit curve reaches the total variance of all test values ($\sigma 2$) or the threshold value, often when it reaches the 95 % threshold of the statistical total variance (Hornschuch and Riek 2009). The threshold value is the difference between the total

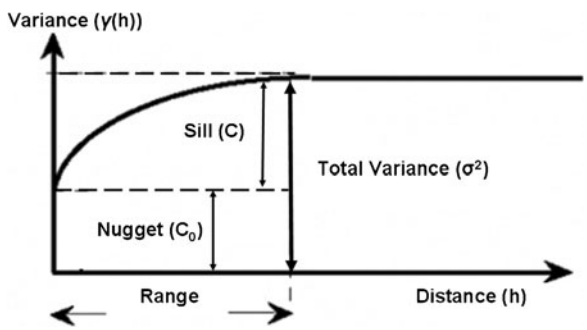

Fig. 7 A spherical semivariogram showing range, still, nugget, and the total variance for a specific lag distance (h)

variance and the nugget effect ($C=\sigma^2-C_0$). The nugget effect (C_0, interface value of the extended best-fit curve with the ordinates) can be understood as non-recorded microvariability or as a measurement error. The nugget effect comprises of the measurement error variance and the small-scale variance within the fields that are less than the smallest observation distance. The threshold value is the maximum value of the semivariogram, which is reached when the measuring values become spatially independent of one another. The range is defined as the distance h, at which the threshold value is reached, i.e., the distance over which measuring values become spatially independent of one another.

Results

The plot scale—long-term monitoring experiments in the laboratory

Analysis of temporal resolution Over a 3-month period from 27 April to 20 July 2009 (DOY 117–210, 84 days), all spectral data (imaging hyperspectal data—AISA-EAGLE and non-imaging from the ASD Spectrometer) as well as vegetation parameter measurements (LAI, Chlorophyll SPAD-502, canopy height, vegetation water content, and C/N content of vegetation) were taken twice a week. The experiment is described in detail above in "Experimental design" section. For spring barley, various vegetation indices were investigated for the AISA-EAGLE imaging spectral data as well as for the ASD non-imaging hyperspectral data with regard to their suitability for the model for various biochemical and biophysical vegetation parameters over the entire vegetation period of 84 days. Figure 8a shows the relationship between the vegetation index NDVI and LAI obtained from laboratory measurements using the imaging spectrometer AISA-EAGLE for spring barley. The color information shows the coincident chlorophyll SPAD-502 content over the entire growing season (DOY 117–201) with NDVI data corresponding to the development and different stages of photosynthetic activity and chlorophyll content (stage I) and the senescence (stage II) of the vegetation.

Very good model results were obtained by implementing the vegetation index GNDVI (R800-R550) from the imaging sensor AISA-EAGLE (Fig. 8b). Here, the LAI could be modeled with an R^2 of 0.83 with a root-mean-square error of 0.70 (Fig. 9). The measurements carried out at the same time under identical conditions (scale 1) with the non-imaging spectrometer ASD (Fig. 8c) over the entire vegetation period of 84 days did not generate any utilizable LAI model result for the vegetation index GNDVI (R800-R550).

The local and regional scale

The statistical LAI model (Fig. 9), obtained from the AISA hyperspectral data from the laboratory observations for the vegetation period of spring barley, then formed the basis of the LAI model derivation for the AISA hyperspectral data with a ground resolution of 1 and 3 m. The results from the LAI modeling can be found in Fig. 10a (LAI-1 m ground resolution) as well as 10b (LAI-3 m ground resolution). The heterogeneity of LAI can on the one hand be clearly seen within the stand of vegetation (Fig. 10a) as well as between the LAI datasets (Fig. 10a, b) with different ground resolutions. The differential image again shows the spatial distribution of differences in LAI with a maximum of ±1.6 between the LAI values derived from the 1 and 3 m hyperspectral data (Fig. 10c).

The investigations on semivariance between LAI-1 m and LAI-3 m (Fig. 10d) show a highly increased variance of the LAI-1 m compared to the LAI-3 m over a lag distance of 50 m. The increased range as well as the total variance σ^2 of LAI for both 1 and 3 m ground resolution can already be recognized from a lag distance of 5 m.

How the spatial characteristics of the NDVI of grassland change with the spatial resolution become apparent in Fig. 11, whereas the areas displaying differences (Fig. 11d–f) between the ground resolutions investigated become more apparent in Fig. 11a–f.

The NDVI for different heterogeneous and structured land uses, grassland, rural vegetation, deciduous forest, and mixed hardwood forest were calculated

Fig. 8 **a** Relationship between the vegetation index NDVI and the LAI obtained from laboratory measurements with the imaging spectrometer AISA-EAGLE for spring barley; **b** Relationship between the vegetation index GNDVI and the LAI obtained from laboratory measurements with the spectrometer ADS for spring barley **c** Relationship between the vegetation index GNDVI and the LAI obtained from laboratory measurements with the imaging spectrometer AISA-EAGLE for spring barley, The color information shows Chlorophyll SPAD-502 content [no dimension] over the entire growing season (DOY 117–201)

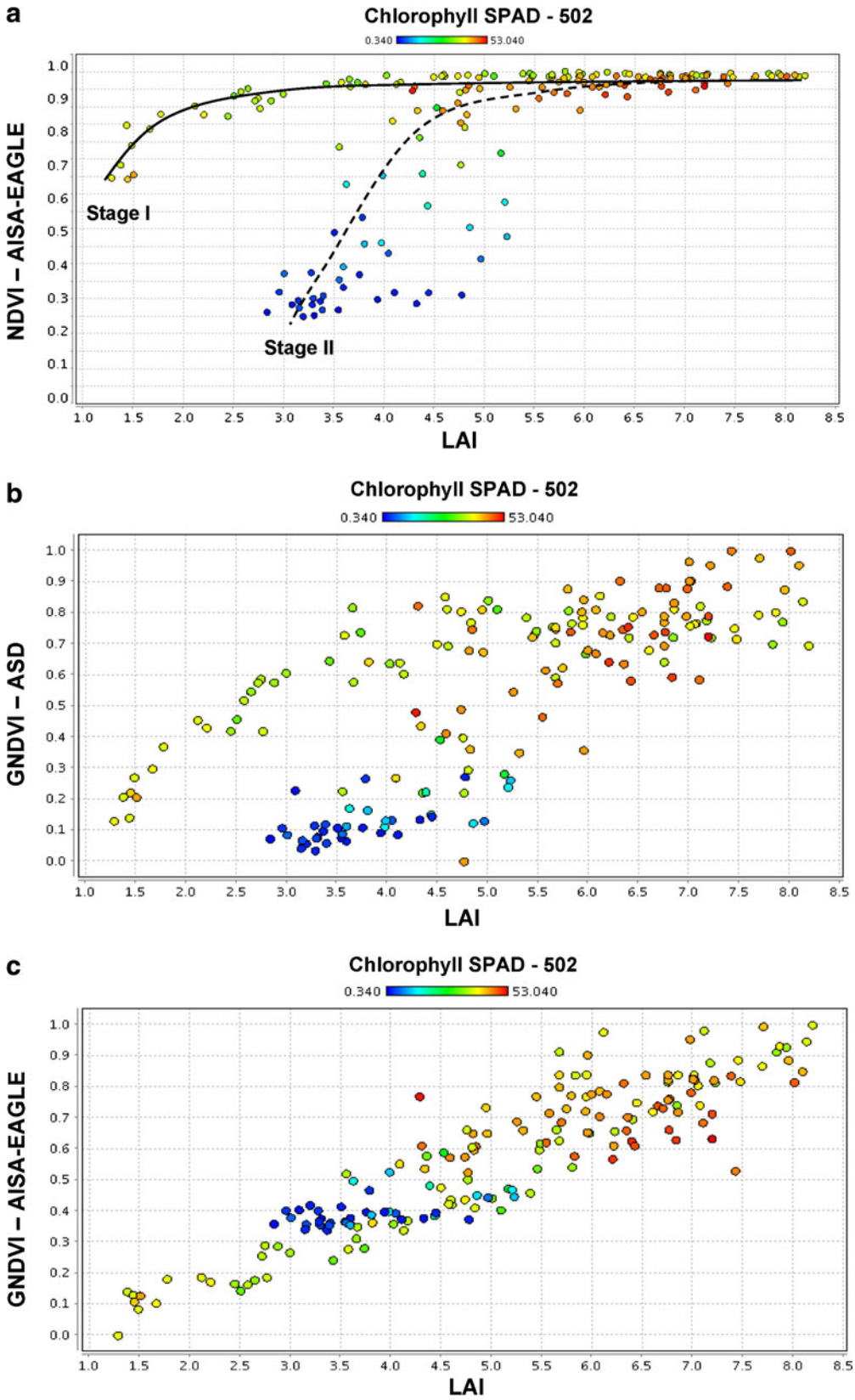
a
Chlorophyll SPAD - 502
0.340
53.040
NDVI – AISA-EAGLE
Stage I
Stage II
LAI
b
Chlorophyll SPAD - 502
0.340
53.040
GNDVI – ASD
LAI
c
Chlorophyll SPAD - 502
0.340
53.040
GNDVI – AISA-EAGLE
LAI

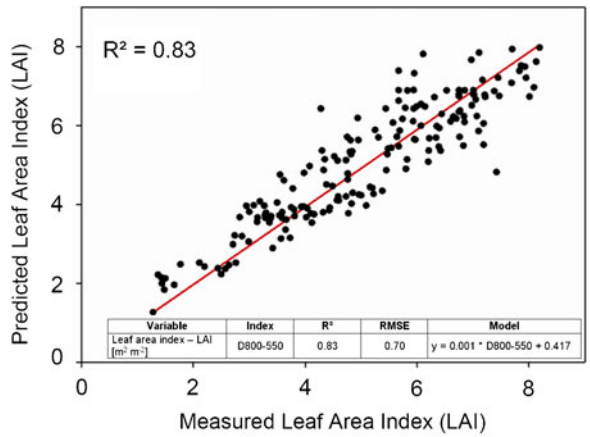

Fig. 9 A comparison between ground LAI measurements and LAI estimates from AISA-EAGLE images using GNDVI (D800-550) for spring barley over an entire growing season (DOY 117–201)

using the hyperspectral data recorded at the different spatial resolutions. To compare the spatial heterogeneities, the statistical variables: median, minimum, and maximum values as well as the semivariance with a lag distance of 50 m were also calculated (Fig. 12a–f).

The median of the NDVI values of the individual land use categories (Fig. 12a–f) only slightly differs between the individual land use categories. For grassland, deciduous forest as well as mixed hardwood forest the median of the NDVI is ~0.8. The differences in calculated NDVI for the different spatial resolutions are marginal (Fig. 12a, c, e, g). Furthermore, for the NDVI of grassland, ruderal vegetation, as well as mixed hardwood forest a high range (minimum, maximum) was calculated, respectively. Only the NDVI for the relatively homogeneous deciduous forest showed a low range for the minimum and maximum values (Fig. 12e).

Due to the semivariance analysis, the spatial characteristics of NDVI for the different spatial resolutions can be compared. As expected the sill for grassland vegetation calculated for the ground resolution of 1 m is higher than for the ground resolution of 2 and 3 m. The semivariance increases considerably up to a lag distance of 10 m, becoming flatter and more constant up to a lag distance of 30 m (Fig. 12b). In spite of the only very slight differences in the average value of the NDVI from 1 to 3 m (Fig. 12a) there are considerable differences in the spatial distribution and the heterogeneity of the NDVI between the three levels of spatial scales investigated (Fig. 12b). The spatial differences in the NDVI distribution increase dramatically up to a lag of 10 m and only slightly from lag 10 to 50 without reaching a stable level.

For land uses, deciduous forest and mixed hardwood forest the semivariance analyses of the NDVI

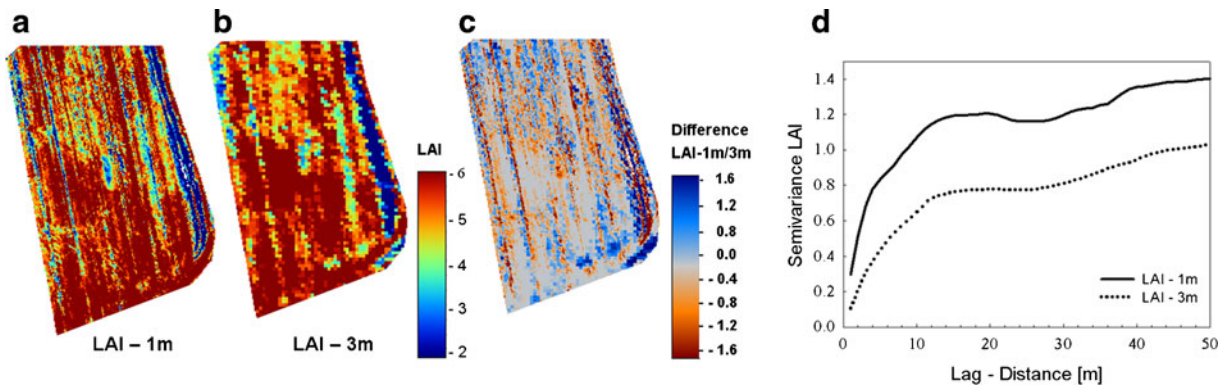

Fig. 10 Thematic map of spatially distributed LAI retrieved from a regression model using AISA hyperspectral images with **a** 1 m ground resolution, **b** 3 m ground resolution, **c** a differential image of LAI 1 m and LAI 3 m, **d** the semivariance for LAI 1 m and LAI 3 m for barley

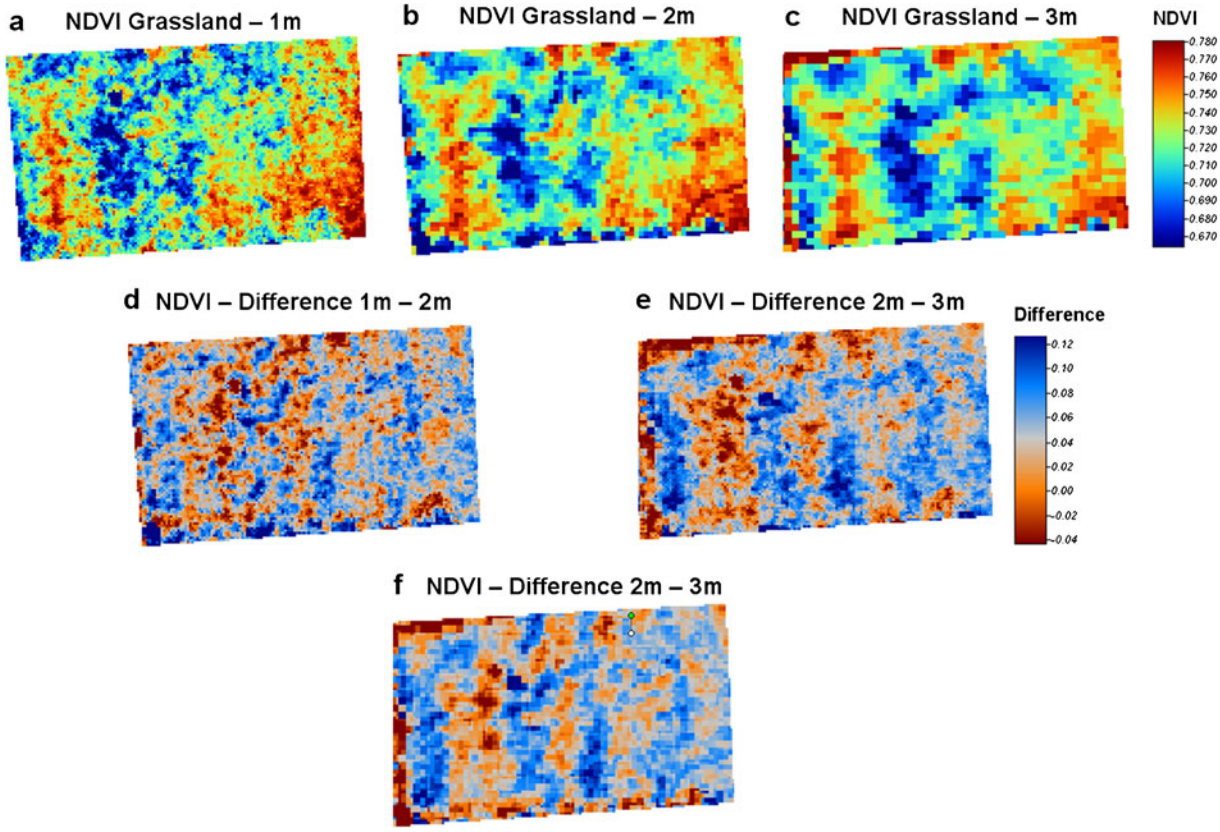

Fig. 11 Calculation of the NDVI from the AISA-EAGLE/HAWK hyperspectral data with different ground resolutions—**a** 1 m, **b** 2 m, **c** 3 m for grassland; Differential images of the NDVI for grassland between **d** 1–2 m, **e** 2–3 m, as well as **f** 2–3 m, date of recording imaging hyperspectral data September 11, 2010

follow a similar pattern to that of grassland (Fig. 12b) for 1, 2, and 3 m (Fig. 10f, h). After an initially sharp increase in the range of variances (1, 2, 3 m) up to a lag distance of 5 m the threshold values become stable up to a lag distance of 50 m. Thus, the variance in the NDVI at 1 m reaches the highest threshold value followed by 2 m. The lowest threshold value is found for the NDVI with a ground resolution of 3 m (Fig. 12f, h). The semivariance analyses of ruderal vegetation (Fig. 12d) show a completely different pattern compared to the results from grassland (Fig. 12b), deciduous forest (Fig. 12f), and mixed hardwood forest (Fig. 12h). Here, the range increases consistently up to a lag distance of 50 m and no stable threshold value is reached. If one compares the curve of the NDVI semivariances of the values from 1, 2, and 3 m resolutions, the NDVI 1 m semivariance increases more greatly compared to the semivariance values of the NDVI from 2 and 3 m (Fig. 12f, h).

Discussion

The plot scale

To examine the causal relationships between hyperspectral imaging signals and the vegetation canopy parameter LAI, controlled laboratory experiments are a very important method for the semi-empirical modeling of the LAI over an entire growing season. Figure 8a shows a hysteresis phenomenon that is typical for vegetation. It can be observed that there is a tendency for the NDVI to level off once it has reached a high level of LAI (LAI>3, DOY 130). The trend indicates a temporary saturation of reflectance, which then disappears with the subsequent senescence of the foliage. This asymptotic behavior has been reported by several authors (Baret et al. 1995; Wiegand et al. 1999). The relationship between LAI and NDVI is a good indicator for the entire phenological evolution of vegetation. For the senescence

period (stage II) of vegetation, dry biomass continued to increase and remained practically constant although the NDVI decreased. If however only the characterization of the development (stage I) of the crop until it reaches a climax is of interest, then the LAI is a good indicator as it shows a significant correlation with the LAI.

The main problem with the use of vegetation indicators is that the vegetation under study can experience changes in biochemical or biophysical characteristics from external disturbance factors such as drought, nutrient stress, or infection. Hence, during the growing season the vegetation will show signs of growing stress. This would mean for example that in phase I a lower NDVI (due to a reduction in chlorophyll) would lead to a misinterpretation of the intermittent process. Due to ancillary and mutually exclusive factors and processes, knowledge is required about the spectral response and its causes over the entire vegetation period. Focused monitoring (scale 1) can help to document additive and counteractive factors and processes of the vegetation and to correctly interpret their spectral response.

As both measurements with the imaging and non-imaging hyperspectral sensors were conducted under the same basic conditions and within a short time interval, it can be assumed that the differences in the model results for the vegetation index GNDVI (R800-R550) are not caused by a change in biochemical or biophysical parameters of the vegetation, soil, or atmosphere, and that thus other factors are influencing the spectral behavior of both sensors. There are several various causes for the different spectral responses of both sensors: (1) differences in sensor-specific mapping characteristics and specific sensor characteristics of the AISA-EAGLE (Whiskbroom–Scanner); (2) the calibration of the non-imaging spectrometer (ASD) with the imaging spectrometer that is sometimes inadequate or not carried out at all. Financial and temporal aspects are often the limiting factors. This leads to uncertainty in the measurements and consequently a reproduction of errors in sensor models and for validation purposes with hyperspectral data (at scales 3 and 4). (3) The inner geometry, structure, and pattern of the vegetation are strongly reflected by the hyperspectral response. This signal is much stronger compared to the spectral response of biochemical and biophysical vegetation parameters (chlorophyll content, vegetation–water content, and protein content). (4) In spite of a comparable FOV from the lenses, both sensors take a different "footprint" of the object to be recorded. (5) If one compares the vegetation index GNDVI over the entire vegetation period of 84 days (DOY 117–201), it becomes obvious that the spectral response for imaging (AISA-EAGLE, Fig. 8c) and non-imaging (ASD, Fig. 8b) hyperspectral sensors takes a very different course from DOY 145. Thus, in addition to the aforementioned influential factors, another factor to be considered is the varying degree of dependency of the spectral signal on a change in phenology.

Fig. 12 *Box plots* for the vegetation index NDVI showing the median, minimum, and maximum values, and outliers for the hyperspectral data recorded by the AISA-EAGLE/HAWK at a 1, 2, and 3 m ground resolution for **a** grassland, **c** ruderal vegetation, **e** deciduous forest, **g** mixed hardwood forest, semivariance of the NDVI for the hyperspectral data recorded by the AISA-EAGLE/HAWK with a 1, 2, and 3 m ground resolution for **b** grassland, **d** ruderal vegetation, **f** deciduous forest, **h** mixed hardwood forest

The local and regional scale

Using the regression model (Fig. 9), the LAI was transformed from the laboratory scale to the local and regional scale to AISA hyperspectral data with a resolution of 1 and 3 m (Fig. 10). As expected, the LAI with a ground resolution of 1 m shows a higher spatially distributed heterogeneity compared to the ground resolution of 3 m. The measured differences in LAI heterogeneity between 1 and 3 m ground resolution (Fig. 10c) cannot be put down to sensor-specific characteristics, due to the fact that the same spectral sensor configurations and process parameters were applied to all data recorded. The LAI heterogeneities for 1 and 3 m hyperspectral data are thus determined by structural factors like for example hydrological as well as characteristics such as grain size, coarseness, types of surface, and structural parameters. Here, the vegetation acts as a "sensor" of patterns and processes in soil and hydrology. The extent of the spatial heterogeneity of soil and hydrological structures and processes is determined by the variability of the spectral response of a pixel.

For the land use structures of grassland, rural vegetation, deciduous forest, as well as mixed hardwood forest, statistical variables were provided and assigned to the box plot. The median values of the NDVI are similar with only slight variation for all land use structures investigated at a spatial resolution of 1, 2, and 3 m. This result differs to the outcome that was achieved with the investigated NDVI range. Here, the land use classes grassland, ruderal vegetation, as well as mixed hardwood forest were given a high value

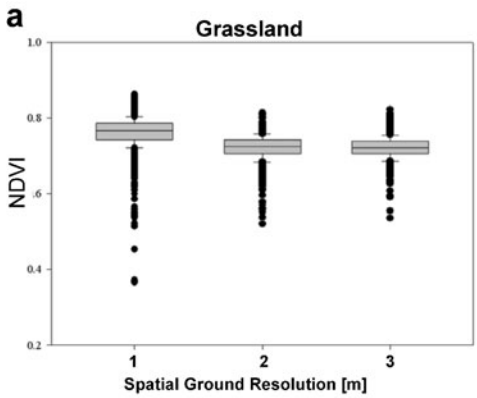
a
Grassland
NDVI
Spatial Ground Resolution [m]

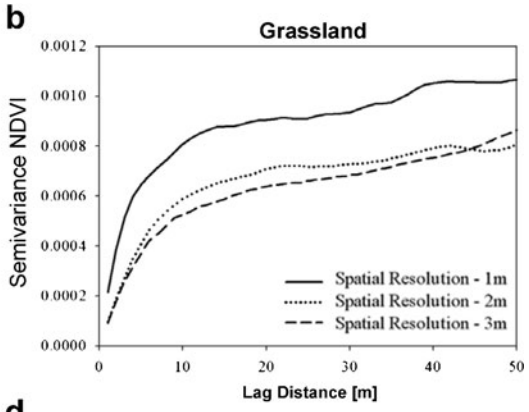
b
Grassland
Semivariance NDVI
Lag Distance [m]
Spatial Resolution - 1m
Spatial Resolution - 2m
Spatial Resolution - 3m

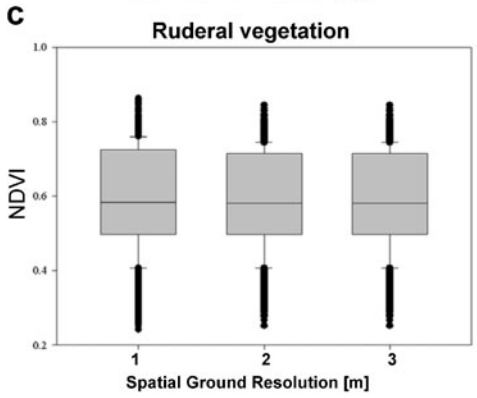
c
Ruderal vegetation
NDVI
Spatial Ground Resolution [m]

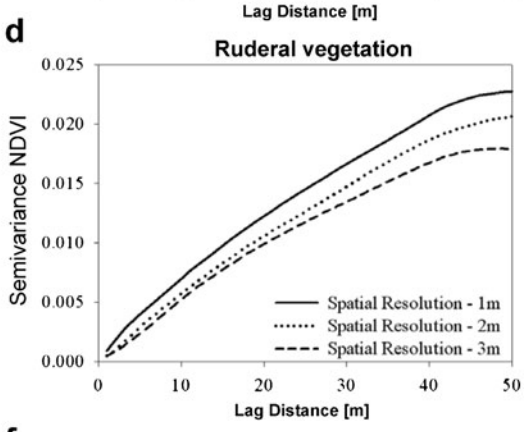
d
Ruderal vegetation
Semivariance NDVI
Lag Distance [m]
Spatial Resolution - 1m
Spatial Resolution - 2m
Spatial Resolution - 3m

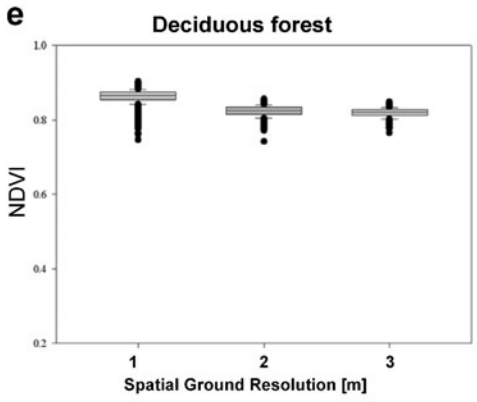
e
Deciduous forest
NDVI
Spatial Ground Resolution [m]

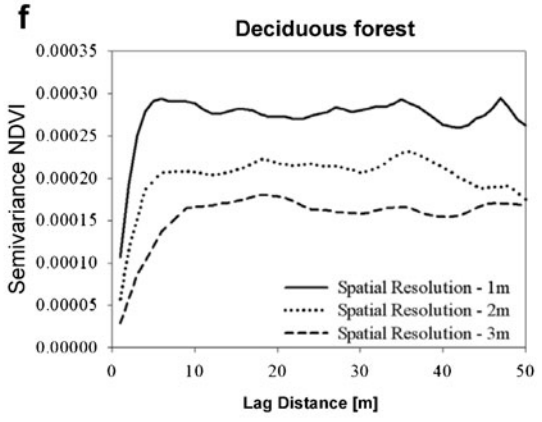
f
Deciduous forest
Semivariance NDVI
Lag Distance [m]
Spatial Resolution - 1m
Spatial Resolution - 2m
Spatial Resolution - 3m

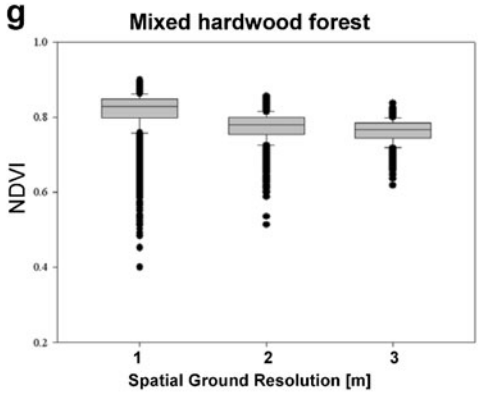
g
Mixed hardwood forest
NDVI
Spatial Ground Resolution [m]

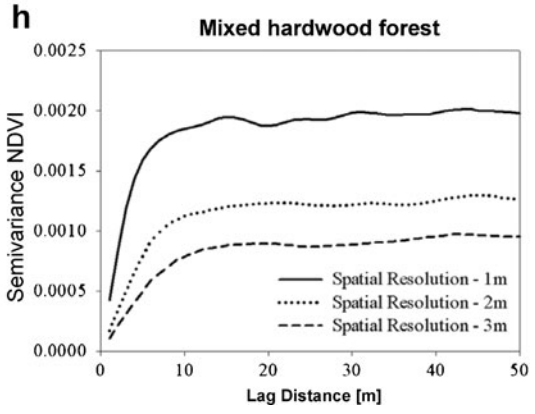
h
Mixed hardwood forest
Semivariance NDVI
Lag Distance [m]
Spatial Resolution - 1m
Spatial Resolution - 2m
Spatial Resolution - 3m

range. It was only for the deciduous forest that the range of minimum and maximum values was very small. The results show that by using simple statistical variables such as the median and the range, statements can already be made about the degree of spatial heterogeneity. A more detailed spatial differentiation of NDVI between the spatial ground resolutions of 1, 2, and 3 m is only possible using geostatistical analyses.

The results of the semivariance analyses of the NDVI of the land use structures investigated at 1, 2, and 3 m ground resolution show a relatively similar trend for the semivariance curves at 1, 2, and 3 m (Fig. 12b, d, f, h). For all land use structures, the variance increases with increasing geometric ground resolution. A decrease in the geometric ground resolution with the same spectral bandwidth can blur the spatial structures that occur at finer spectral resolutions.

Relatively homogeneous land uses such as grassland, homogenous deciduous forest, and mixed hardwood forest up to a lag distance of ca. 10 m display a high sill which then reaches a constant threshold. This semivariance trend of the different land use structures indicates a small-scale existent trend of NDVI values (Hornschuch and Riek 2009). By contrast, the NDVI semivariance of ruderal vegetation is exponential, i.e., an obvious range or threshold value cannot be recognized. This indicates that the patterns are very large-scale and difficult to separate (Hornschuch and Riek 2009). Wu et al. (2000) analyzed the semivariance of a boreal forest region based on a Landsat TM scene (1984). He was able to prove a similar spherical trend in the semivariance for a boreal forest region.

Conclusions and outlook

Why does a controlled long-term laboratory experiment need to be conducted on the plot scale? The spectral response of the sensor depends on the physiological conditions of the vegetation. In the literature, there are a number of spectral vegetation indices, which are used to describe the variables of physiological processes such as LAI, chlorophyll, photosynthetic activity, or the water content of vegetation. The development of these indices came about on the one hand from the implementation of physical-based models and from long-term monitoring investigations by means of a non-imaging spectrometer (ASD). Both approaches are criticized in the following way: (1) in using a physical model (i.e., SAIL or PROSPECT), a very precise characterization and parameterization of the geometrical and biochemical characteristics of plants is required. The validation of landscape models using an imaging spectrometer (i.e., HyMap, airborne hyperspectral sensor, 126 spectral bands, wavelength interval of 0.45–2.5 μm) or a non-imaging spectrometer (i.e., ASD) is considered to be very complex due to overlaying processes in the landscape (i.e., stress from drought and nutrient stress). (2) Long-term ASD measurements in the field are only possible under certain conditions due to limited radiation days in the year as well as the environmental variables of the vegetation such as soil moisture, temperature, and radiation that can only be measured in situ. It can be assumed that the collection of ASD spectra over a long-term vegetation period is very difficult to achieve. (3) Therefore, it is important to measure land surface vegetation variables with one imaging optical sensor over the whole vegetation period. These measurements are necessary for understanding the interaction between spectral response and vegetation change for the calibration of airborne hyperspectral image data and field validation.

Why are flights important to record different spatial resolutions?

The results from the hyperpsectral imagery that we recorded at the different geometric resolutions of 1, 2, and 3 m show that the similarity or heterogeneity of the vegetation indices derived such as the NDVI changes according to the spatial resolution. These changes depend on the heterogeneity and the dynamics of the underlying processes and structures such as the soil structure, the soil moisture, and matter fluxes etc. It will therefore be the goal of further analyses to determine these factors and transfer functions between different scales. Here, it is important not only to look at the spectral characteristics of the vegetation at a given point in time, but also to integrate land structure and dynamics as well as hydrological properties.

Why is the OSADIS approach at hand promising for investigating scales?

The objective of applying this method is to combine hyperspectral remote sensing data on different spatial

and temporal scales to investigate the potential of using one hyperspectral sensor data as an input for the local, regional, and landscape scale. The use of only one hyperspectral sensor on different temporal and spatial scales offers the unique opportunity to compare data on different spatial scales as well as transfer the process information obtained from monitoring investigations in the field.

Our first results enabled us to show that it is not only possible to combine sensors with different characteristics (e.g., AISA EAGLE, HyMap, and ASD) in a geometrical spectral and temporal manner but also to use these process investigations over different scales.

With our OSADIS approach, we seem to be "*taking one step* back" in an attempt to nevertheless better understand scales, structures, patterns, and their temporal changes and to be able to describe and quantify them.

The comparison of measuring instruments with different imaging optics and sensors is extremely challenging and a true calibration of imaging and non-imaging hyperspectral sensors before flights and measurements is often not carried out due to financial and technical restrictions. Spectral sensors have (1) different imaging characteristics, (2) spectral and spatiotemporal imaging characteristics as well as FOV. (3) In an attempt to conform these, BRDF occurs as well as type-specific spectral responses, resulting from differences in sensors as opposed to differences in processes.

By implementing the OSADIS approach, we are able: (a) to develop suitable stress-controlled long-term vegetation indices for selected variables such as the LAI, chlorophyll, photosynthesis, water content, nutrient content, etc; (b) to transfer the models obtained to the landscape level; (c) to record imaging hyperspectral information on different spatial scales, achieving a true comparison of the structure and process results; (d) to minimize existing errors from geometrical, spectral, and temporal effects due to sensor and time-specific differences; and (e) to carry out a true top- and downscaling by determining scale-dependent correction factors and transfer functions.

Acknowledgments The research was funded and supported by Terrestrial Environmental Observatories (TERENO), which is a joint collaboration program involving several Helmholtz Research Centers in Germany. The authors wish to thank all technicians for their continuous support at all levels.

References

Bannari, A., Khurshid, K. S., Staenz, K., & Schwarz, J. W. (2007). A comparison of hyperspectral chlorophyll indices for wheat crop chlorophyll content estimation using laboratory reflectance measurements. *IEEE Transactions on Geoscience and Remote Sensing, 45*, 3063–3074.

Baraldi, A., Durieux, L., Simonetti, D., Conchedda, G., Holecz, F., & Blonda, P. (2010). Automatic spectral-rule-based preliminary classification of radiometrically calibrated SPOT-4/-5/IRS, AVHRR/MSG, AATSR, IKONOS/QuickBird/OrbView/GeoEye, and DMC/SPOT-1/-2 Imagery—part I: system design and implementation. *IEEE Transactions on Geoscience and Remote Sensing, 48*, 1326–1354.

Baret, F., Clevers, J. G. P. W., & Steven, M. D. (1995). The robustness of canopy gap fraction estimates from red and near-infrared reflectances: a comparison of approaches. *Remote Sensing of Environment, 54*, 141–151.

Carter, G. (1994). Ratios of leaf reflectances in narrow wavebands as indicators of plant stress. *International Journal of Remote Sensing, 15*, 697–703.

Chen, C.-M., Hepner, G. F., & Forster, R. R. (2003). Fusion of hyperspectral and radar data using the IHS transformation to enhance urban surfaces. *ISPRS ISPRS—International Society for Photogrammetry and Remote Sensing, 58*, 19–30.

Dennison, P. E., & Roberts, D. A. (2003). Endmember selection for multiple endmember spectral mixture analysis using endmember average RMSE. *Remote Sensing of Environment, 87*, 123–135.

Dungan, J. L. (2001). Scaling up and scaling down: the relevance of the support effect on remote sensing of vegetation. In N. J. Tate & M. P. Atkinson (Eds.), *Modelling Scale in Geographic Information Science*. Chichester: Wiley.

Ettema, C. H., & Wardle, D. A. (2002). Spatial soil ecology. *Trends in Ecology & Evolution, 17*, 177–183.

Gascon, F., Gastellu-Etchegorry, J. P., Lefevre-Fonollosa, M. J., & Dufrene, E. (2004). Retrieval of forest biophysical variables by inverting a 3-D radiative transfer model and using high and very high resolution imagery. *International Journal of Remote Sensing, 25*, 5601–5616.

Gastellu-Etchegorry, J. P., Martin, E., & Gascon, F. (2004). DART: a 3D model for simulating satellite images and studying surface radiation budget. *International Journal of Remote Sensing, 25*, 73–96.

Gibson, C. C., Ostrom, E., & Ahn, T. K. (2000). The concept of scale and the human dimensions of global change: a survey. *Ecological Economics, 32*, 217–239.

Gitelson, A. A., Kaufmann, Y. J., & Merzylak, M. N. (1996). Use of a green channel in remote sensing of global vegetation from EOS-MODIS. *Remote Sensing of Environment, 58*, 289–298.

Gobron, N., Belward, A. S., Pinty, B., & Knorr, W. (2010). Monitoring biosphere vegetation 1998–2009. *Geophysical Research Letters, 37*, 0148–0227.

Guanter, L., Segl, K., & Kaufmann, H. (2009). Simulation of optical remote-sensing scenes with application to the EnMAP Hyperspectral Mission. *IEEE Transactions On Geoscience And Remote Sensing, 47*, 2340–2351.

Haboudane, D., Miller, J. R., Tremblay, N., Zarco-Tejada, P. J., & Dextraze, L. (2002). Integrated narrow-band vegetation indices for prediction of crop chlorophyll content for application to precision agriculture. *Remote Sensing of Environmental, 81*, 416–426.

Haboudane, D., Tremblay, N., Miller, J. R., & Vigneault, P. (2008). Remote estimation of crop chlorophyll content using spectral indices derived from hyperspectral data. *IEEE Transactions on Geoscience and Remote Sensing, 46*, 423–437.

Hornschuch, F., & Riek, W. (2009). Bodenheterogenität als Indikator von Naturnähe? 2. Biotische und abiotische Diversität in Natur- und Wirtschaftswäldern Brandenburgs und Nordwest-Polens. *Waldökologie Landschaftsforschung und Naturschutz, 7*, 55–82.

Isaak, E. H., & Srivastava, R. M. (1989). *An introduction to applied geostatistics*. New York, USA: Oxford University Press.

Jacquemoud, S., Verhoef, W., Baret, F., Bacour, C., Zarco-Tejada, P. J., Asner, G. P., et al. (2009). PROSPECT +SAIL models: a review of use for vegetation characterization. *Remote Sensing of Environment, 113*, 56–S66.

Li, S., Kwok, J. T., & Wang, Y. (2002). Using the discrete wavelet frame transform to merge Landsat TM and SPOT panchromatic images. *Information Fusion, 3*, 17–23.

Li, Q., Hu, B., & Pattey, E. (2008). A scale-wise model inversion method to retrieve canopy biophysical parameters from hyperspectral remote sensing data. *Canadian Journal of Remote Sensing, 34*, 311–319.

Lillesand, T. M., & Kiefer, R. W. (1994). *Remote sensing and image interpretation*. New York: Wiley.

Mäkisara, K. (1998). AISA data user's guide, Technical Research Centre of Finland. *Research Note, 1894*, 1–54.

Mäkisara, K., Meinander, M., Rantasuo, M., Okkonen, J., Aikio, M., Sipola, K., et al. (1993). Airborne Imaging Spectrometer for Applications (AISA). *Digest of IGARSS'93, 2*, 479–481. Tokyo, Japan.

Malenovský, Z., Bartholomeus, H. M., Acerbi-Junior, F., Schopfer, J. T., Painter, T. H., Epema, G. F., et al. (2007). Scaling dimensions in spectroscopy of soil and vegetation. *International Journal of Applied Earth Observation and Geoinformation, 9*, 137–164.

Meentemeyer, V. (1989). Geographical perspectives of space, time, and scale. *Landscape Ecology, 3*, 163–175.

Metternicht, G. I., & Zinck, J. A. (2003). Remote sensing of soil salinity: potentials and onstraints. *Remote Sensing of Environment, 85*, 1–20.

Myneni, R. B. (1991). Modeling radiative-transfer and photosynthesis in 3-dimensional vegetation canopies. *Agricultural and Forest Meteorology, 55*, 323–344.

Myneni, R. B., & Ganapol, B. D. (1991). A simplified formulation of photon transport in leaf canopies with scatterers of finite dimensions. *Journal of Quantative Spectroscopy & Radiative Transfer, 46*, 135–140.

Painter, T. H., Dozier, J., Roberts, D. A., Davis, R. E., & Green, R. O. (2003). Retrieval of subpixel snowcovered area and grain size from imaging spectrometer data. *Remote Sensing of Environment, 85*, 64–77.

Quattrochi, D. A. (1993). The need for a lexicon of scale terms in integrating remote-sensing data with geographic information-systems. *Journal of Geography, 92*, 206–212.

Ranchin, T., Aiazzi, B., Alparone, L., Baronti, S., & Wald, L. (2003). Image fusion-the ARSIS concept and some successful implementation schemes. *ISPRS ISPRS—International Society for Photogrammetry and Remote Sensing, 58*, 4–18.

Richter, R., & Schlapfer, D. (2002). Geo-atmospheric processing of airborne imaging spectrometry data. Part 2: atmospheric/topographic correction. *International Journal of Remote Sensing, 23*, 2631–2649.

Rogaß, C., Spengler, D., Bochow, M., Segl, K., Lausch, A., Doktor, D., et al. (2011). Reduction of radiometric miscalibration—applications to pushbroom sensors. *Sensors, 11*, 6370–6395. doi:10.3390/s110606370.

Rouse, J. W., Haas, R. H., Schell, J. A., & Deering, D. W. (1973). Monitoring vegetation systems in the Great Plains with ERTS. In *Proceedings of Third Earth Resources Technology Satellite Symposium* (Vol. 1, pp. 309–317). Washington, DC: NASA. Goddart Space Flight Center.

Saunders, S. C., Chen, J., Drummer, T. D., Gustafson, E. J., & Brosofske, K. D. (2005). Identitying scales of pattern in ecological data: a comparison of lacunarity, spectral and wavelet analysis. *Ecological Complexity, 2*, 87–105.

Schönermark, M. V., Geiger, B., & Roser, H. P. (2004). *Reflection properties of vegetation and soil*. Berlin: Wissenschaft und Technik.

Segl, K., Guanter, L., Kaufmann, H., Schubert, J., Kaiser, S., Sang, B., et al. (2010a). Simulation of spatial sensor characteristics in the context of the EnMAP Hyperspectral Mission. *IEEE Transactions on Geoscience and Remote Sensing, 48*(7), 3046–3054.

Segl, K., Guanter, L., Kaufmann, H., Schubert, J., Kaiser, S., Sang, B., et al. (2010b). Simulation of spatial sensor characteristics in the context of the EnMAP Hyperspectral Mission. *IEEE Transactions on Geoscience and Remote Sensing, 48*, 3046–3054.

Sellers, P. J. (1985). Canopy reflectance, photosynthesis and transpiration. *International Journal of Remote Sensing, 6*, 1335–1372.

Silvan-Carrdenas, J. L., & Wang, L. (2010). Retrieval of subpixel Tamarix canopy cover from Landsat data along the Forgotten River using linear and nonlinear spectral mixture models. *Remote Sensing of Environment, 114*, 1777–1790.

Smith, M. O., Johnson, P. E., & Adams, J. B. (1985). Quantitative determination of mineral types and abundances from reflectance spectra using principal component analysis. *Journal of Geophysical Research, 90*, 797–804.

Tarnavsky, E., Garrigues, S., & Brown, M. E. (2008). Multiscale geostatistical analysis of AVHRR, SPOT-VGT, and MODIS global NDVI products. *Remote Sensing of Environment, 112*, 535–549.

Tuia, D., Pacivici, F., Kanevski, M., & Emery, W. J. (2009). Classification of very high spatial resolution imagery using mathematical morphology and support vector machines. *IEEE Transactions on Geoscience and Remote Sensing, 47*, 3866–3879.

Verhoef, W. (1984). Light scattering by leaf layers with application to canopy reflectance modeling: the SAIL model. *Remote Sensing of Environment, 16*, 125–141.

Volk, M., & Ewert, F. (2011). Scaling methods in inegrated assessment of agriculatural system—state-of-the-art and future directions. *Agriculture, Ecosystems and Environment, 142*, 1–5.

Webster, R., & Oliver, M. A. (2001). *Geostatistics for environmental scientists. Statistics in practice*. Chichester: Wiley.

Wiegand, T., Moloney, K. A., Naves, J., & Knauer, F. (1999). Finding the missing link between landscape structure and population dynamics: a spatially explicit perspective. *The American Naturalist, 154*, 605–627.

Wu, J. (2009). Scale issues in remote sensing: a review on analysis, processing and modeling. *Sensors, 9*, 1768–1793. doi:10.3390/s90301768.

Wu, J., Jelinski, D. E., Luck, M., & Tueller, P. T. (2000). Multiscale analysis of landscape heterogeneity: scale variance and pattern metrics. *Geographic Information Sciences, 6*, 6–19.

Zacharias, S., Bogena, H., Samaniego, L., Mauder, M., Fuß, R., Pütz, T., et al. (2011). A network of terrestrial environmental observatories in Germany. *Vadose Zone Journal, 10*, 955–973.

Zeng, Y., Schaepman, M. E., Wu, B., Clevers, J. G. P. W., & Bregt, A. K. (2009). Quantitative forest canopy structure assessment using an inverted geometric-optical model and up-scaling. *International Journal of Remote Sensing, 30*, 1385–1406.

Zhou, J., Civco, D. L., & Silander, J. A. (1998). A wavelet transform method to merge Landsat TM and SPOT panchromatic data. *International Archives of Photogrammetry and Remote Sensing, 19*, 743–757.